Ancient TL

www.ancienttl.org · ISSN: 2693-0935

Issue 22(2) - December 2004
https://doi.org/10.26034/la.atl.v22.i2

Design of a blue LED stimulation unit with a highly uniform illumination pattern

I. Quesada, M.R. Otazo, L. Baly* and Y. Gonzalez

Centro de Aplicaciones Tecnológicas y Desarrollo Nuclear (CEADEN) AP 6122, Miramar, La Habana, Cuba.
(*Corresponding author: baly@ceaden.edu.cu)

(Received 11 November 2004; in final form 8 December 2004)

Abstract
The current study is concerned with the design and construction of a blue LED stimulation unit with a highly uniform illumination pattern. The pattern produced by a single LED is characterized experimentally. Using this information and making certain approximations, the illumination pattern produced by an array of LEDs was computer generated, and the mean intensity and relative standard deviation were calculated. In this way, several hypothetical configurations were evaluated; the most convenient configuration was constructed and experimentally characterized. The measured uniformity expressed as the relative (to the mean intensity) standard deviation in the sample zone was as good as 1.7%.

Introduction
Quartz photoluminescence is being widely employed for dating and retrospective dosimetry. This has encouraged the development of reliable reading systems, with emphasis on improvements in the detection system, the stimulation unit, the electronics and the ionizing radiation source. The stimulation unit is an essential part of any photoluminescence reading system and it should supply radiation with an appropriate power density that is both spectrally and temporally stable. With such an aim halogen lamps, ultra-bright green and blue LEDs (Bøtter-Jensen, 2000: Bøtter-Jensen and Murray, 1999: Bøtter-Jensen et al., 1999) and more recently, solid state lasers (Duller et al., 2000) have been employed. Figure 1 shows the standard configuration used to measure the photoluminescence; a photomultiplier tube faces a sample of quartz crystals that are spread over a 1cm-diameter metallic disk.

Ultra-bright LEDs have several advantages over other classes of light sources. They have the features of a solid state device such as compactness, robustness, long life, low power consumption and low cost. Compared with ultra-bright green LEDs, blue LEDs are more efficient at producing photoluminescence (Bøtter-Jensen, 2000) and thus they have been extensively studied for this application (Bøtter-Jensen and Murray, 1999; Bøtter-Jensen et al., 1999). These studies demonstrated the high spectral and temporal stabilities of these devices. The selection of the specific arrangement of the LEDs has been guided mainly by the requirement of producing a given power density at the sample.

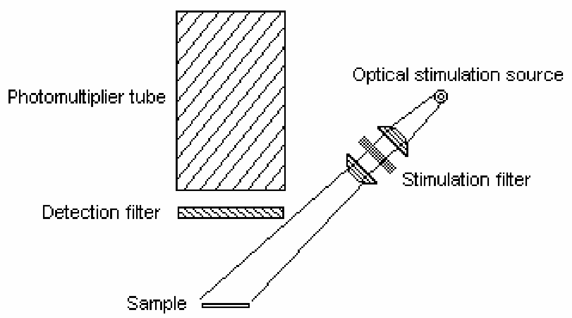

Figure 1: *Standard configuration of a photoluminescence reading system*

Recent reports have drawn attention to the fact that only a small percentage of quartz crystals show effective photoluminescence (Duller et al., 2000; Jacobs et al., 2003). In the case of multi-crystal samples, these bright crystals are randomly distributed in the sample holder and their exact position will be different every time the position of the sample disc is changed on the holder. This may become a serious source of variability if the pattern of illumination at the sample is not uniform. Since the luminescence signal is determined by the intensity of the stimulation radiation received by each crystal, the luminescence signal will depend on the position of these bright crystals in relation to the illumination pattern.

In the present work, the design of a blue LED stimulation unit is described, and in addition to the general requirements, special significance is given to the production of a highly uniform illumination pattern. To achieve this, the illumination pattern of a single LED was experimentally characterized, and these data were used to develop a computer code to generate the illumination pattern of an hypothetical array of LEDs. For each generated pattern, the mean intensity and standard deviation (uniformity) were calculated, and several configurations were evaluated. The most convenient configuration was constructed and experimentally characterized.

Starting design considerations

The power density of typical configurations based on blue LEDs has been reported to be in the range of 20 - 40 mW/cm^2 (Bøtter-Jensen, 2000) and the current stimulation unit is planned to produce similar levels of power density. The illumination uniformity will be evaluated as the relative standard deviation of the radiation intensity across the sample. At the moment, there is no strong criterion that leads to the selection of uniformity; however, a 10% standard deviation will be taken as the guiding parameter.

First, the performance characteristics of a blue LED were analyzed. The maximal power emitted by an ultra-bright blue LED is about 2 mW; thus, a minimum number of 20 LEDs will be needed to match the highest power density reported in the literature. Second, the illumination pattern produced by a single LED is not uniform. Notable differences between the intensities at the spot center and the borders are observed (Figure 2). Therefore, even when several LEDs are arranged appropriately, producing a highly uniform pattern seems to be complicated.

Proposed solution

To resolve this problem, sample illumination using only part of the illuminated area will be used. The boundaries of such a region will be determined by a cut-off relative intensity; in our case, this region is defined by the points whose intensity is higher than 0.9 I_{max}, hereafter the 90% cut-off region.

To implement such an idea, two problems need to be solved. First the distance between the LED and the sample, for which the sample will be illuminated with the 90% cut-off region, should be determined. Unfortunately, the viewing angle reported by the LED manufacturer corresponds to the 50% cut-off region, and can not be used for our purposes. Therefore, a detailed study of the illumination pattern for different distances between the LED and the sample should be made.

Second, under the new conditions the power delivered to the sample will be less than the total one, and therefore, the percentage of the total power contained within the 90% cut-off region needs to be found. This parameter will be important for determining the number of LEDs required to achieve the planned power density.

Experimental

Figure 3 shows the experimental setup employed to characterize the illumination pattern. The LED was fixed to a variable length arm and a photodiode with a 0.3 mm-diameter collimator was mounted in a dual axis X-Y micropositioning system. An electronic module attached to the system allowed the reading of the photodiode position with a precision of 10 µm.

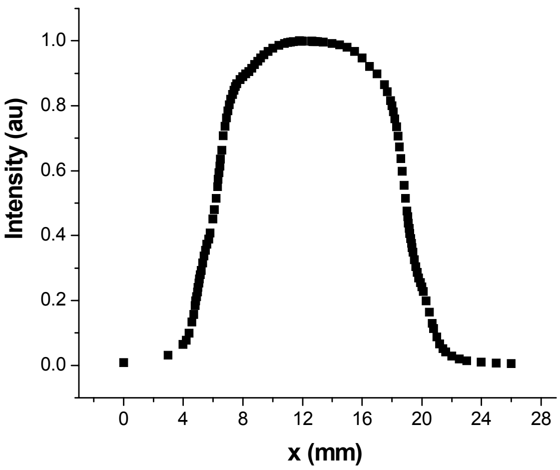

Figure 2: *Illumination pattern produced by an ultra-bright blue LED.*

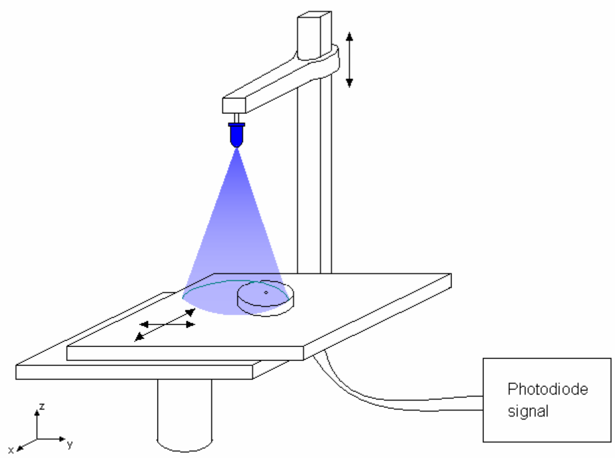

Figure 3: *Experimental setup to measure the illumination pattern of a single LED.*

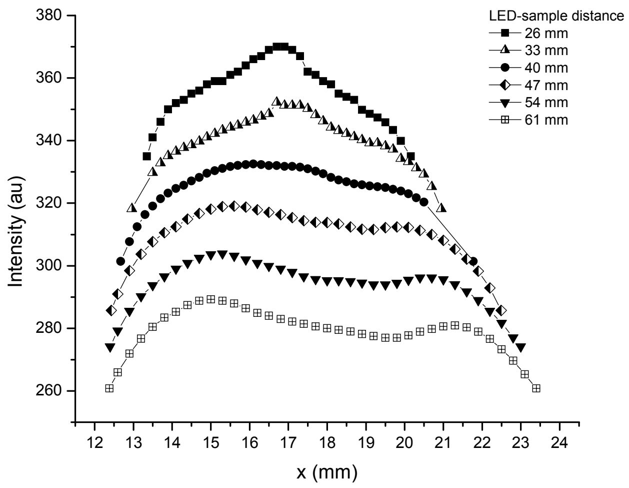

Figure 4: *Measured distribution of intensity in a single axis for different distances between the LED and the photodiode.*

Figure 4 shows the measured distribution of intensity in a single axis for different distances (from 26 mm to 61 mm) between the LED and the photodiode; note that only the 90% cut-off region is shown. From these data, a new graphic (Figure 5) was constructed to reflect the dependence of the geometrical width of several cut-off regions for different distances between the LED and the photodiode.

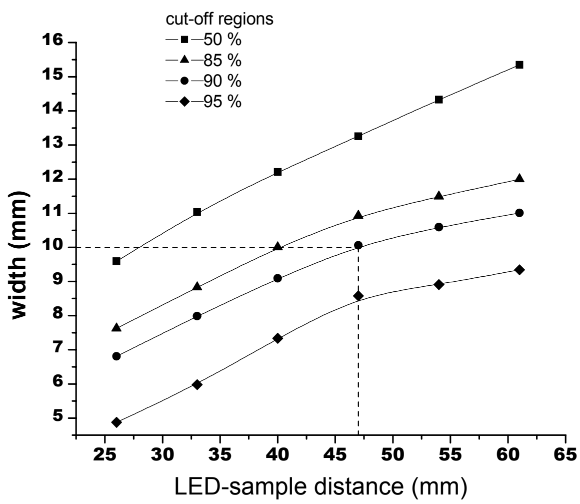

Figure 5: *Geometrical width of several cut-off regions for different distances between the LED and the photodiode.*

Finally, from the experimental data, the percentage of the power contained in each cut-off region for different distances was calculated (Figure 6). The percentage was determined as the ratio of the area included in the cut-off region to the whole distribution area.

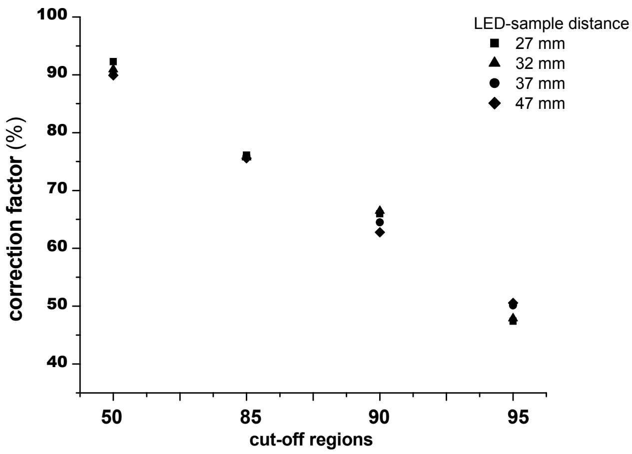

Figure 6: *Power correction factor in each cut-off region for different distances.*

At this point some important conclusions can be presented:

1. For a normal angle of illumination and a distance of 47 mm between the LED and the 10 mm diameter sample, the latter is totally illuminated by the 90% cut-off region, as shown by the lines drawn in Figure 5. When the distance is less, the sample area is not illuminated with greater than 90% of maximal power.
2. Under these conditions, the power delivered to the sample will be approximately 60% of the total (Figure 6).
3. Considering a sample area of 0.78 cm^2 (i.e. with diameter of 10 mm) illuminated by the 90% cut-off region and a maximal output power for a blue LED of 2 mW, the planned power density of 40 mW/cm^2 in the sample zone will be reached with a minimum of 26 LEDs.

Procedure for the pattern generation of the LED configuration

The next step in the construction of the stimulation units is the selection of the LED configuration. The LED configuration is defined by the number of LEDs, their orientation and distribution, but the number of possible configurations is huge.

The application of an empirical method to select the best configuration has several drawbacks. First, the mechanical support for the LEDs is difficult to construct as a flexible test rig, and second, there is no procedure for the evaluation in advance of the sample illumination uniformity. Instead, we chose to compute the illumination pattern produced by an hypothetical array of LEDs and then selected the most suitable configurations using a program based on the MatLab 5.3 code.

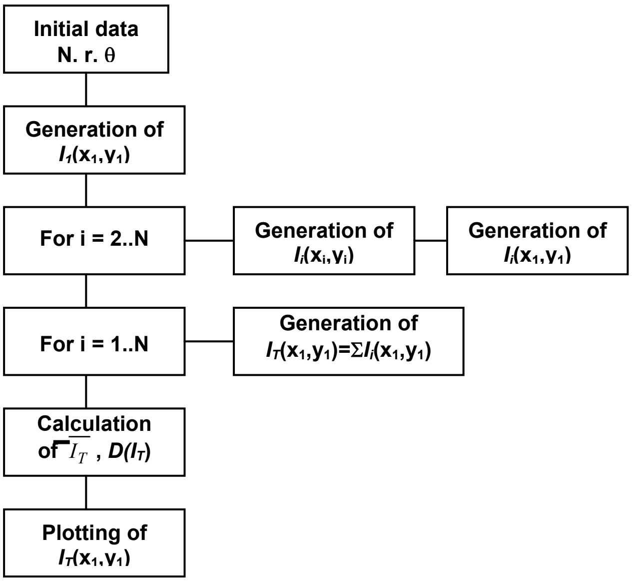

Figure 7: *General algorithm used to generate the illumination pattern of an array of LEDs.*

Figure 7 shows the general algorithm used to generate the illumination pattern of an array of LEDs. First, the pattern of the first LED $I_1(x_1,y_1)$ is computer generated. Then, the pattern of the following LED $I_i(x_i,y_i)$ (i= 2..N) is generated and interpolated to the coordinate system of the first LED $I_i(x_1,y_1)$. This procedure is performed for each LED after which the array pattern I_T is calculated by summing all individual patterns $I_i(x_1,y_1)$ (i= 1..N). Finally, the mean intensity $\overline{I_T}$, and the standard deviation $D(I_T)$ are calculated for later comparison.

Single LED pattern generation module

From this algorithm, it can be seen that the single LED pattern generation plays an important role. The heart of this module is a sub module whose function is to calculate the radiation intensity at any point within the space limited by the following conditions: –7 mm < x < 7 mm, –7 mm < y < 7 mm, 47 mm < z < 61 mm, where z is the distance between the LED and the sample when the illumination is performed at a normal angle. To calculate the intensity, this sub module uses the intensity distribution measured with a space resolution Δx = Δy = 0.3 mm in three different planes A(z=47), B(z=54) and C(z=61) (Figure 8). Then assuming that for every pair x,y the intensity varies linearly as z, the intensity at any point I(x,y,z) is calculated as the linear interpolation of I(x,y,zA), I(x,y,zB) and I(x,y,zC).

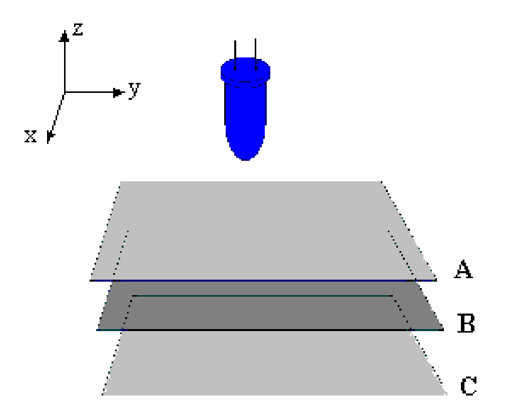

Figure 8: *Schematic representation of the three geometrical planes where the intensity was measured.*

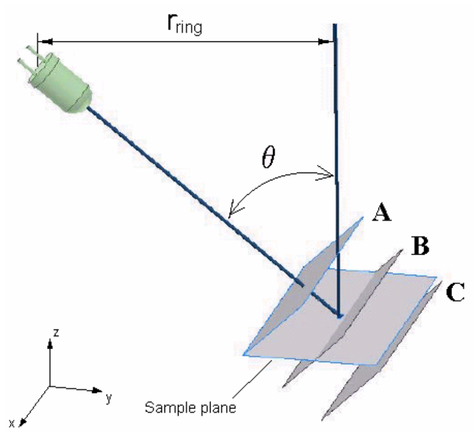

Figure 9: *Schematic representation of the three geometrical planes where the intensity was measured in relation to the sample plane.*

There is a second sub module which, depending on the LED position and orientation, determines the points of the sample plane in the LED coordinate system (Figure 9). For calculations it is considered that the LED is aligned parallel to the y axis and that the interception of such a line with the sample plane occurs at x = 0. The origin of the sample coordinate system is located on its center. The LED position and orientation is defined by two parameters: the angle θ and the distance r; the first is the angle between the normal to the sample plane and the direction of the LED alignment, the second is the LED y-coordinate. After introducing the parameters θ and r, this module checks that such a combination is geometrically consistent with the requirement that the distance between the sample and the LED is 47 mm. When successful, it generates the illumination pattern produced by such an LED in the sample plane.

Selection of the LED configuration

Figure 10 shows the model that was used for each evaluated configuration. The LEDs are distributed in two concentric rings of 20 LEDs each. The total number of LEDs (40) is higher than previously calculated; however, in this configuration the LEDs will not be subjected to extreme operating conditions. Each ring is characterized by its radius r and angle θ.

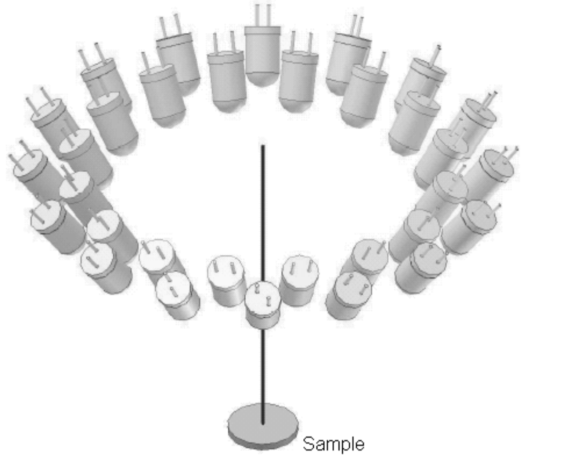

Figure 10: *Model for the evaluated positions.*

Using the design program AUTOCAD and considering the minimal distance between the LED and the sample as well as the dimensions of the photomultiplier tube, the range of possible values for the radius of the ring was determined. Starting from r = 22 mm and incrementing the radius in steps of 0.5 mm, a set of radii was defined. For each predefined radius r and different values of θ, the pattern produced by each ring was generated and visually evaluated. The mean intensity and the standard deviation were also calculated. For each radius, the angle θ producing the pattern with the smallest standard deviation was selected. Once again, using the program AUTOCAD, proposed configurations were evaluated, but this time considering the real LED dimensions. From this analysis two configurations were selected (Table 1).

r(mm)	θ	$D(I_T)$	$\overline{I_T}$	I_T max	$I_T(0,0)$
28.0	32.0	2095.1	95642	98711	98658
35.0	39.5	1484.7	95171	97073	97073

Table 1: *Parameters of the two selected configurations.*

Construction and evaluation of the stimulation unit

Using the results of the previous section, the stimulation unit was designed and constructed (Figure 11). Before the LEDs were mounted, the power output of each LED was determined (Figure 12) and they were found to vary by up to 30%. To minimize any effects, LEDs with similar outputs were mounted in the inner ring; the rest were mounted in the outer ring, alternating one LED of low output with another one of high output.

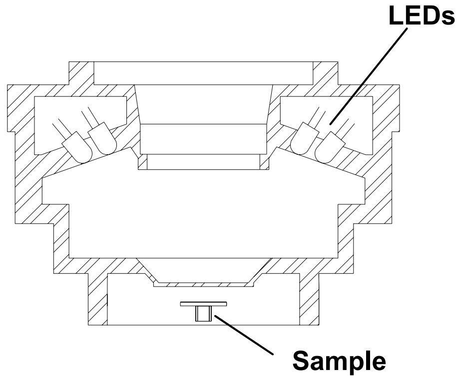

Figure 11: *Layout of the stimulation unit.*

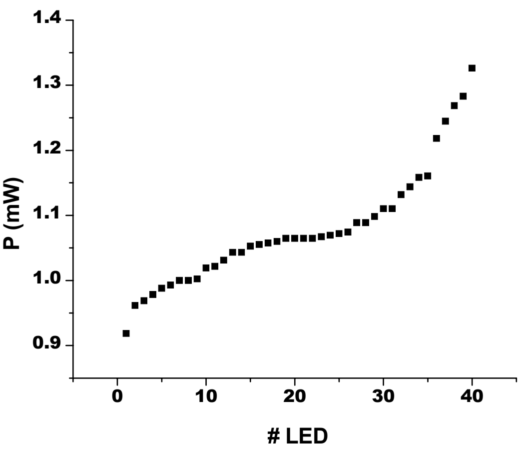

Figure 12: *Power output of the 40 LEDs employed in the stimulation unit.*

To characterize the stimulation unit, it was mounted in the experimental setup (Figure 3) and the illumination pattern was measured (Figure 13). Prior to the measurement, the linearity of the photodiode response had been verified. Figure 14 shows the same data truncated out of the sample zone, where it is observed that the pattern is almost flat. The calculated standard deviation in the sample zone was as low as 1.7 %, which is several times lower than the planned uniformity.

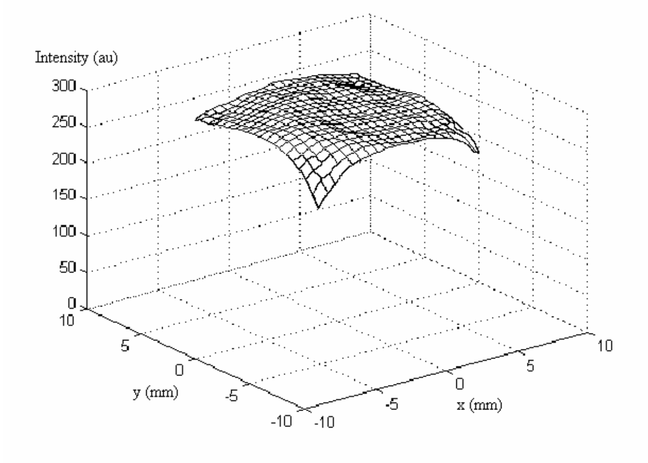

Figure 13: *Measured illumination pattern in the sample plane.*

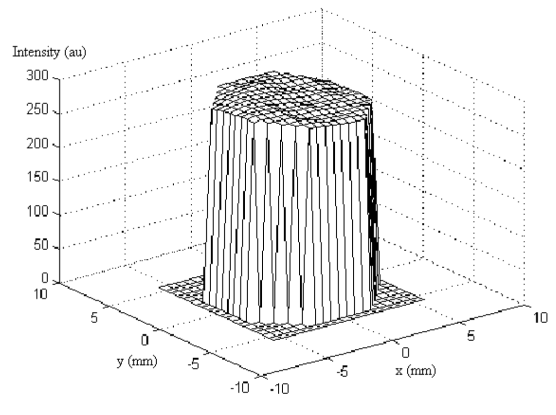

Figure 14: *Measured illumination pattern in the sample zone.*

Conclusions

A blue LED stimulation unit with a highly uniform illumination pattern was designed and constructed, following the development of a computational tool to allow minimization of the experimental work.

References

Bøtter-Jensen L. (2000) *Development of optically stimulated luminescence techniques using natural minerals and ceramics, and their application to Retrospective Dosimetry*. Risø National Laboratory Risø-R-1211(EN), 185 pp.

Bøtter-Jensen L., Murray A. S. (1999) Developments in optically stimulated luminescence techniques for dating and retrospective dosimetry. *Radiation Protection Dosimetry* **84**, 307-316.

Bøtter-Jensen L., Duller G. A. T., Murray A. S., Banerjee D. (1999) Blue light emitting diodes for optical stimulation of quartz in retrospective dosimetry and dating. *Radiation Protection Dosimetry* **84**, 335-340.

Duller G.A.T., Bøtter-Jensen L., Murray A.S. (2000) Optical dating of single sand-sized grains of quartz: sources of variability. *Radiation Measurements* **32**, 453-457.

Jacobs Z., Duller G. A. T., Wintle A. G. (2003) Optical dating of dune sand from Blombos Cave, South Africa: II –single grain data. *Journal of Human Evolution* **44**, 613-625.

Reviewer

Ann Wintle

Red luminescence emission from potassium feldspars stimulated by infrared

Morteza Fattahi[1,2], Stephen Stokes[2] and Michel Lamothe[3]

1. The Institute of Geophysics, Tehran University, Kargar Shomali, Tehran, Iran.

2. Oxford Luminescence Research Group, School of Geography and the Environment, University of Oxford, Mansfield Road, Oxford OX1 3TB.

3. Département des Sciences de la Terre et de l'Atmosphere, Université du Québec à Montreal, C.P. 8888, Succ. Centre-Ville, Montréal, Québec, Canada H3C 3P8

(Received 23 June 2004; in final form 18 January 2005)

Abstract

The use of the blue–UV Infrared stimulated luminescence (IRSL) from feldspars in luminescence dating has generally been unsuccessful due to age underestimation related to anomalous fading. The red emission from feldspar may however provide a non-fading alternative. A series of experiments are reported here which investigate IR stimulated (λ = 833 ± 5 nm) red luminescence emission from potassium feldspar. The aim is to demonstrate the potential of red IRSL as an alternative to the widely used UV-blue emission IRSL approaches. Five key factors are optimised to increase the dose-related red IRSL signal, and to decrease the background signal levels. These include photomultiplier tube (PMT) characteristics, detection filter combinations, laser diode intensity, measurement temperature, and substrate related effects. Preliminary measurements are described that illustrate the considerable potential of red IRSL for dating applications, including low sensitivity changes from volcanic potassium feldspars and high dose saturation of red IRSL from sedimentary and volcanic potassium feldspars.

Keywords

Luminescence dating; feldspar; red emission; infrared; orange- red IRSL

Introduction

Huntley et al. (1985) demonstrated the possibility of obtaining an optically stimulated luminescence (OSL) signal from feldspar, and the use of OSL in dating applications is now well established. Hütt et al. (1988) published the first optical stimulation spectrum for feldspar showing a large stimulation peak in the near IR (825-1030 nm). This unexpected stimulation peak in the near infrared for feldspars was confirmed in later studies and by a number of authors (see Table 4 and Figure 9 of Duller, 1997; Wintle, 1997; Krbetschek et al., 1997).

The IR stimulated luminescence emission spectra vary considerably round the ternary feldspar compositional diagram (Duller, 1997). Krbetschek et al. (1997) reported emission bands at 280, 330, 410, 560 and 700 nm for the IRSL of potassium-rich feldspars extracted from sediment samples. With respect to signal detection, the commonly used EMI 9635Q PMT is biased towards detection in the blue-violet range with 25% quantum efficiency at 400 nm, around six times higher than that at 570 nm. Luminescence workers have used this capability primarily for the detection of blue-violet potassium feldspar emissions (e.g. Duller, 1994a,b, 1997).

Due to several potential advantages, including the speed of resetting of the luminescence clock by exposure to sunlight (Li and Wintle, 1994), the use of IRSL for dating sediments has attracted considerable attention. However, despite over a decade of research, satisfactory agreement with independent age control has been shown only in a few studies (e.g. young samples in Duller, 1994b; Clarke et al. 1996). In particular, the application of infrared stimulation blue luminescence (IRSL) has been hampered by anomalous fading and the associated problem of age underestimation (e.g. Balescu et al., 2001; Huntley and Lamothe 2001; Lamothe and Auclair, 1997, 1999, 2000; Lian and Shane, 2000; Richardson et al., 1997, 1999; Spooner, 1992, 1994; Wallinga et al., 2000).

Zink and Visocekas (1997) have shown that red (which they termed near-IR) ($\lambda >$ 590 nm) thermoluminescence (RTL) of at least some species of feldspar do not suffer from anomalous fading, whereas blue emissions ($\lambda <$ 590 nm) from identical samples do exhibit the effect. They demonstrated that RTL emission in sanidine feldspar possessed a number of characteristics similar to that of the blue range emission. These included similarities in activation energies and sensitivity to sunlight bleaching, with both signals bleaching rapidly in a few hours of exposure. Fattahi (2001) has shown that orange-near red IRSL (λ = 600-660 nm) shows either no or less anomalous fading in comparison with UV IRSL for the feldspar samples examined. A logical extension of these works would be, as has been the case for UV-blue emission of both quartz and feldspar, to establish whether it is possible to observe the red emission under optical stimulation and if so, determine whether red IRSL possesses similar or different characteristics in comparison to UV-blue IRSL. Technological difficulties in developing a system which is capable of detecting in the red, while rejecting other wavelengths, have restricted further research in this area (Duller, 1997). The primary technical limitation in red IRSL detection is the potentially high background of the measurement system. This background is mainly due to two sources: reflection of the incident IR stimulation photons, and thermal incandescence.

Given its potential to circumvent anomalous fading, we consider the development of a suitable detection system and the testing of IR stimulated red emissions to be a priority for luminescence dating and one which we have systematically evaluated (Fattahi, 2001). As with conventional OSL of quartz and IRSL of feldspars, practical advantages in exploiting anti-Stokes radiation encouraged us, in combination with the well-known feldspar stimulation IR resonance, to first consider the use of IR stimulation wavelengths to detect a red emission.

This and a companion paper (Fattahi and Stokes, 2003b) present results of our attempts to assemble suitable optics and maximise an infra-red stimulated red luminescence emission from feldspar. Our ultimate aim is to validate the signals as routine integrating dosimeter for dating purposes.

In this paper we use ‘‘ Red’’ as a name to describe all detection windows used in this study between 600-720 nm; ‘‘IRSL’’ as a name to describe the conventionally employed UV-blue IRSL ($\lambda_{emission}$ < 600 nm); ‘‘orange- red IRSL’’ to describe IRSL in the wavelength emission region c. 600-720 nm; “orange-near-red IRSL” to describe IRSL in the wavelength emission range 600-660 nm; and “far-red IRSL’’ to describe IRSL in the wavelength emission range 665-720 nm.

Experimental conditions

A full description of our experimental apparatus is given in Fattahi and Stokes (2003b) and only a summary is provided here. Experiments were carried out using a Risø TL-DA-15 automated TL/OSL system (fitted with a $^{90}Sr/^{90}Y$ beta source delivering ~7 Gy.min^{-1}). Three photomultiplier tubes were used. These consisted of either an Electron Tubes 9635Q (hereafter called the “blue”) tube, or one of two cooled (T ~ -20°C), extended range PMTs: an Electron Tubes D716A (hereafter called the “green” tube) bialkaline PMT; or an Electron Tubes 9658 (hereafter called the “red” tube) S20 PMT, that are equipped with an S 600 PHOTOCOOL thermo-electric refrigeration chamber which allows active cooling of the photocathode down to 40°C below room temperature.

The system incorporates a powerful focused IR laser diode stimulation source, which provides incident photon energy of up to ~ 400 mW.cm^{-2} at the sample, at a wavelength of 833 ± 5 nm. Luminescence was measured through filter combinations designed to transmit a variety of broad (λ= 590-720 nm) or narrower (λ = 600-660 nm λ = 665-720 nm) red emissions (Fattahi and Stokes, 2003b).

The potassium feldspar samples used in this study were collected from a variety of geographical locations. Sample (OX_{OD} 847/5) is a late Holocene New Zealand dune sand. Sample 99/5/1 is a Mid Pleistocene New Zealand Ignimbrite. Four samples were obtained from terrace deposits in the Upper Loire Valley, France (15/1, 15/2, 14/1 and 21/1), kindly provided by Alison Colls. A fluvioglacial sample from Ontario (Middle Wisconsinan deposits near St. Thomas, Ontario, Canada with Laboratory identification: Y7A). Six further samples were obtained from UAE (WW1A, 2A, 3A, 4A, 1B and WW2B).

Optimisation of the IRSL (>600 nm) emission

We identify five main parameters that affect the signal and background: sample temperature including thermal incandescence, intensity of the IR stimulation source, IR reflection of substrate surface, and PMT and filter combination characteristics. We have considered the effect of these parameters individually, and in combination, for efficient red IRSL detection.

The effect of sample temperature and IR laser diode intensity on background

It is obvious that the probability of eviction of electrons from traps depends on the intensity of the stimulation source. Different models have been suggested for the production of IRSL in feldspar, including a thermally–assisted photon process (Hütt et al., 1988; Trautmann et al., 2000; Poolton et al., 2002a,b). However, the amount of thermal assistance is strongly dependent upon the optical excitation energy chosen (Poolton et al, 2002a). Doubling the stimulation power will double the rate of arrival of photons and therefore the luminescence emitted per unit time from a given trap (Aitken, 1998). Increasing the sample temperature (stimulation temperature) will also increase the eviction of electrons. According to Aitken (1998), near room temperature this eviction rate increases by the order of 1% per degree centigrade. Increasing the stimulation temperature and light intensity therefore has the advantage, for dim samples, of increasing the signal relative to the background due to PMT noise. The potential disadvantages of increasing the IR diode intensity and sample temperature can be divided in two categories. Firstly, the background will increase, with temperature and photon flux, which are themselves due to thermal incandescence and reflection of stimulating photons from a sample. Secondly, thermal quenching, if present, decreases the luminescence centres efficiency as the temperature is increased (e.g. Poolton et al., 1995). As such, our attention has focused on minimising thermal incandescence and reflected stimulation photon flux.

Thermal incandescence has previously hampered the application of the red emission in thermoluminescence dating (e.g. Fattahi and Stokes, 2001; 2003a). The effect of IR reflection originating from a typical 1W infrared (830 ± 5 nm) laser diode unit is an order of magnitude greater than the effect of thermal incandescence (c. 10^{-2} J.m^{-3}) at ~ 500°C at 900 nm, as a background component (Fattahi and Stokes, 2003b).

To explore the effect of IR laser diode intensity on background, we have examined a variety of substrate types while varying the laser intensity (0-100%). For this experiment we used four disks: two aluminum (Al) disks, one of which was painted black (using a marker), and two stainless steel (SS) disks, one of which was again painted black. Figure 1 demonstrates that there is a significant IR intensity-related background signal. It is additionally noted that at higher IR intensities there is an initial small decay component in this background, which is probably related to IR source characteristics. This feature requires further investigation. Figure 2 compares the typical effect of the laser intensity at 30%, 60% and 90% on the 4 disks. Similar patterns are observed for other filter combinations and PMT (but with background intensities varying from some millions to only 100 counts per second). Clearly background represents a significant issue in red IRSL detection system design.

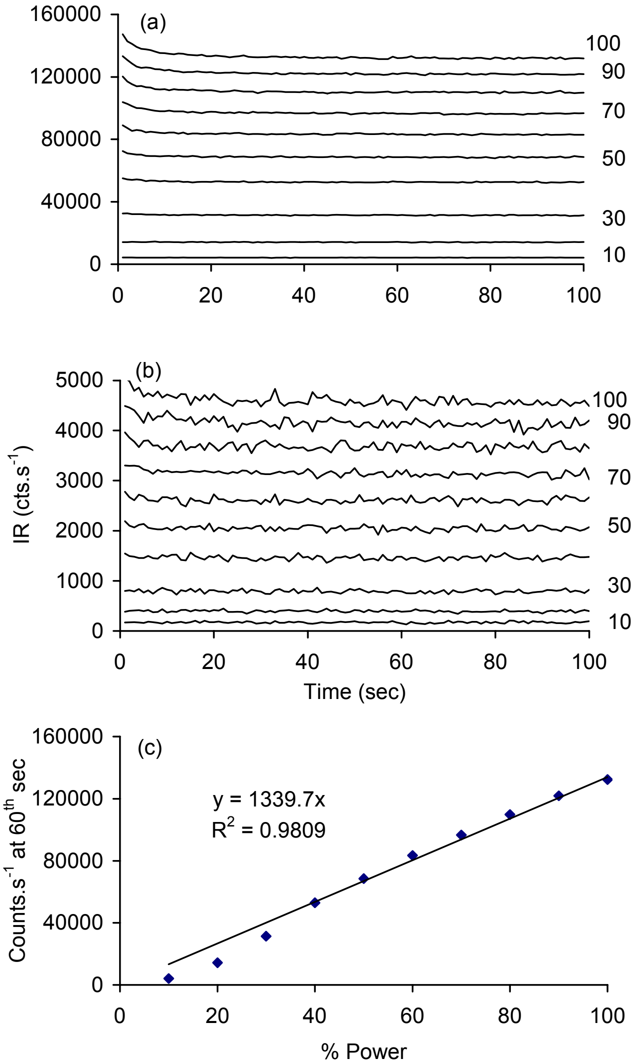

Figure 1: *Reflected IR from a blank stainless steel disk using red PMT and two sets of filter combinations. (a) Omega 740 SP + FR 400S + OG590, (b) Omega 740 SP + 2*FR 400S + OG590. (c) Relationship between the IR counts and laser out put of figure (a). The labels on the data lines give the intensity (% of maximum) of IR laser output. In all groups of filter combinations examined, the same pattern has been observed.*

The widely employed Pilkington HA-3 heat rejection filter used in UV-blue TL and OSL studies cannot prevent the IR transmission in red luminescence studies using a conventional "blue" bialkali PMT (Figure 2a). This confirms previous results reported by Fattahi and Stokes (2000).

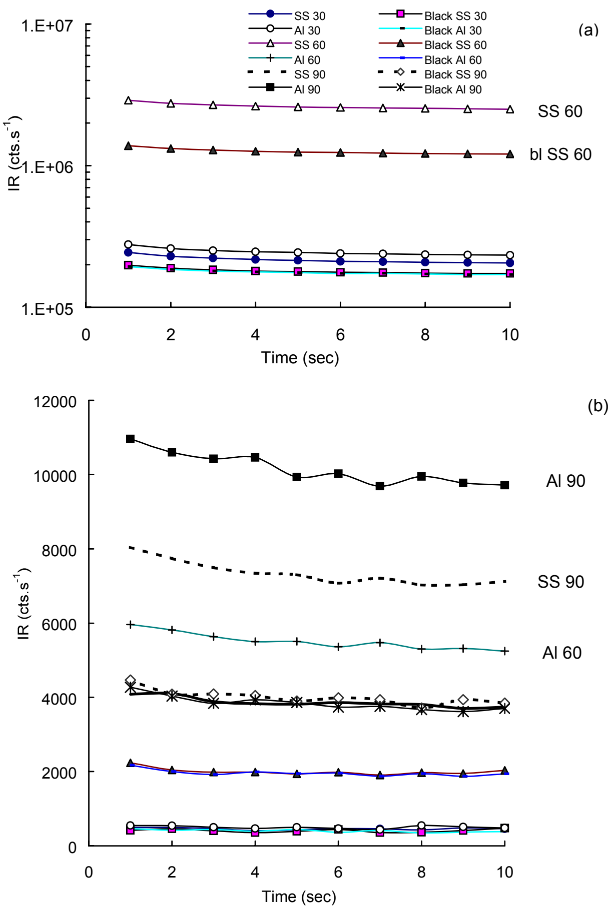

Figure 2: *Reflected IR from, two aluminium (Al) disks, and two stainless steel (SS), one of which is painted black, using two filter combinations. (a) For HA3 + OG 590. (b) For FR 400S + OG 590. The labels on the data lines give the disk used and the intensity (% of maximum) of IR laser output.*

A combination of Omega 740 SP + Corion FR 400S + OG 590 and the "red" PMT decrease the background at 100% laser intensity from > 10^6 to ~1.5 x 10^5 cts.s^{-1} (Figure 2a). Addition of another FR 400S reduces it to ~5 x 10^3 cts.s^{-1}.

Some combinations of IR cut filters are able to decrease the background from in excess of millions of counts per second to a low level comparable to PMT dark noise (a few hundred counts per second). The general pattern noted is that reflected IR is high for both unpainted Al and stainless steel substrate, the former consistently being greater. The levels of IR reflection are clearly related to the IR intensity (Figure 2b). However, when the disk surfaces are painted black, while a background dependence on IR intensity remains, we obtain considerably lower backgrounds (at least half) than for the unpainted discs, and there is no significant difference observed between the two substrate types, as expected. This suggests that further investigation is required to find a substrate that is more suitable for red-IRSL measurements than aluminium or stainless steel. Didier Miallier (personal communication) has investigated that a stainless steel disk that has been exposed to air for a while will always give a significant spurious signal when heated; for circumventing this effect, the disk must be preheated once shortly before a set of measurements.

For some filter combinations, background levels were as low as 100-200 cts.s^{-1} but the signals are correspondingly lower and this limits potential dating applications. A key observation is that background is mainly due to the reflection of incident light, which is directly related to the IR source intensity. In comparison, the PMT dark count is negligible. Therefore, the optimum configuration for red IRSL measurement is use of a substrate with minimum IR reflection, while applying the maximum IR intensity.

The effect of filter and PMT combinations on red IRSL measurements

A range of filter combinations and PMTs was tested using sample 847/5 (Fattahi, 2001). The result demonstrated that each PMT needs a specific filter combination to optimise the signal and signal to noise, and comparing three PMTs with a single filter combination will not demonstrate the optimum results for all tubes.

While there is at present no definitive choice, we consider the green PMT in combination with two FR 400S plus OG 590 or RG 665 as an efficient arrangement for detection of red IRSL decay curves over a broad red emission range (~ 600-720 nm) or far-red (~ 665-720 nm) of spectrum, respectively. An Omega 625DF50 alone, in combination with the green PMT, is suitable in cases where details of the entire decay form and low background levels are required in orange-near-red (~ 600-660 nm) part of the spectrum. If a green PMT is not available, we suggest the red PMT in combination with two FR 400S + BG 39 (1mm) plus OG 590 or RG 665 for detecting of orange-red or far-red IRSL decay curves, respectively. Alternatively, for very bright samples if neither the red or green PMT are available, an Omega 625DF50 or Omega 750 SP + OG590 filters combined with a blue PMT may provide a usable combination for orange-near red portion of the spectrum. The combination of Omega 750 SP + RG665 filters and a blue PMT may provide a usable combination for far-red IRSL detection. While this would result in a very low signal yield, it has the advantage of not requiring active cooling.

Suggestions for stimulation source investigations

The most significant contribution to the background signal is from the IR source, due to the close position of the detection (600–720 nm) and stimulation (~ 830 nm) wavelengths and high intensity of the IR laser. Figure 3 shows the characteristics of the IR laser source used for this study. In our opinion the short tail of the IR laser wavelength has an enormous effect on background.

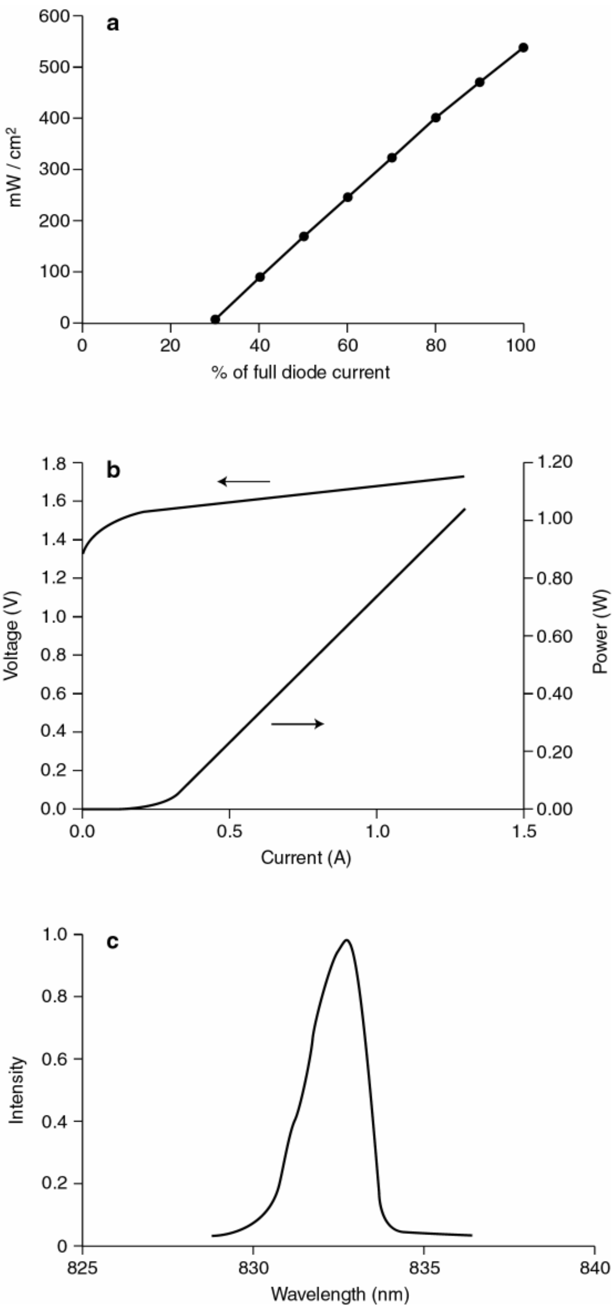

Figure 3: *HPD1110-9mm IR laser characteristics. (a) from Risø catalogue. (b) and (c) from High Power Devices catalogue.*

A variety of IR-cut filters (employed in this study) have been used to reduce the background from IR laser source. But, these filters have also reduced signal detection efficiency from samples. Therefore, the use of IR-cut filters has not satisfied both high signal level and signal-to-noise ratio. There are two alternatives for increasing the signal to noise and reducing the background. Firstly, we suggest using another laser diode that stimulates at higher wavelengths (i.e., > 850 nm). Secondly, we suggest the use of a combination of long-pass (short-cut) and interference filters in front of the HPD1110-9 mm IR laser.

An examination of some basic red IRSL and RTL properties of potassium feldspar

Figure 4 shows the typical stimulation and detection bands used for the following section of this study.

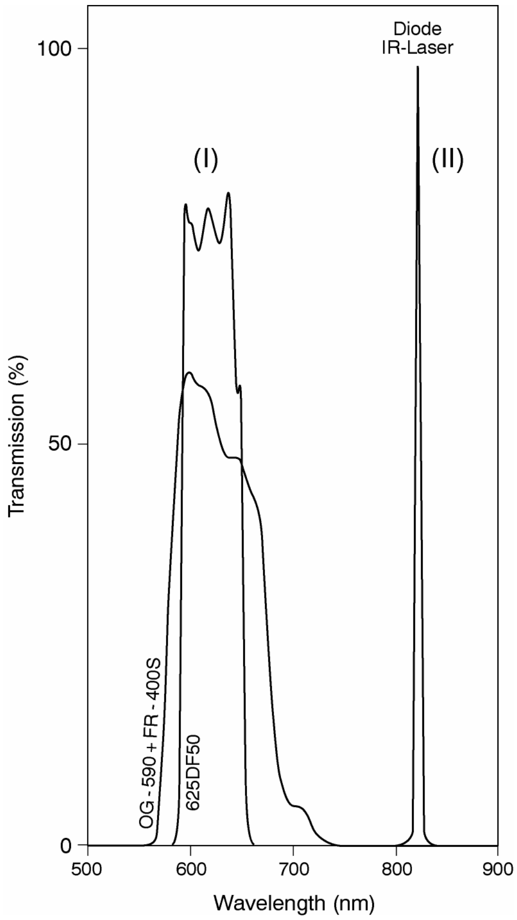

Figure 4: *The stimulation (II) and detection (I) bands used in this study. (I) Transmission through detection filters (Omega 625DF50 and a combination of OG590 + FR 400S). (II) IR stimulation source spectrum (833 ± 5 nm).*

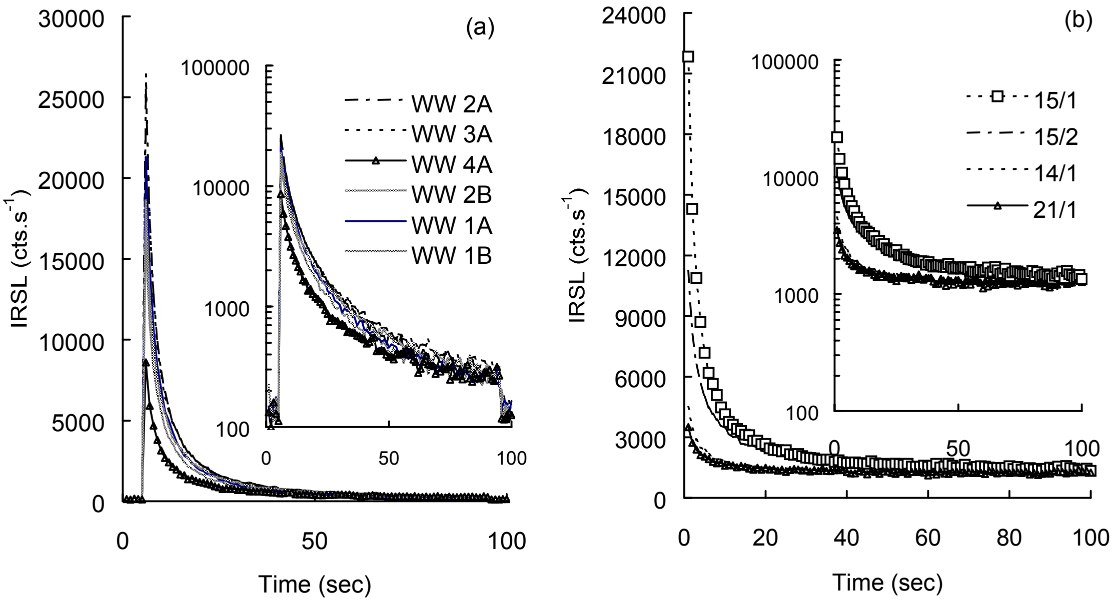

Figure 5: *Natural red IRSL decay curves (pre-heated at 250°C for 60 s) of feldspar samples collected from UAE (WW 1-4A and WW 1-2B) and France (15/1, 15/2, 14/1 and 21/1), respectively. (a) UAE samples detected through EMI 9635Q "Blue" tube and OG 590 + BG 39, inset shows the same curves on a logarithmic y-axis scale. (b) French samples detected through D716A "Green" PMT and RG 665 + FR 400S + BG 39.*

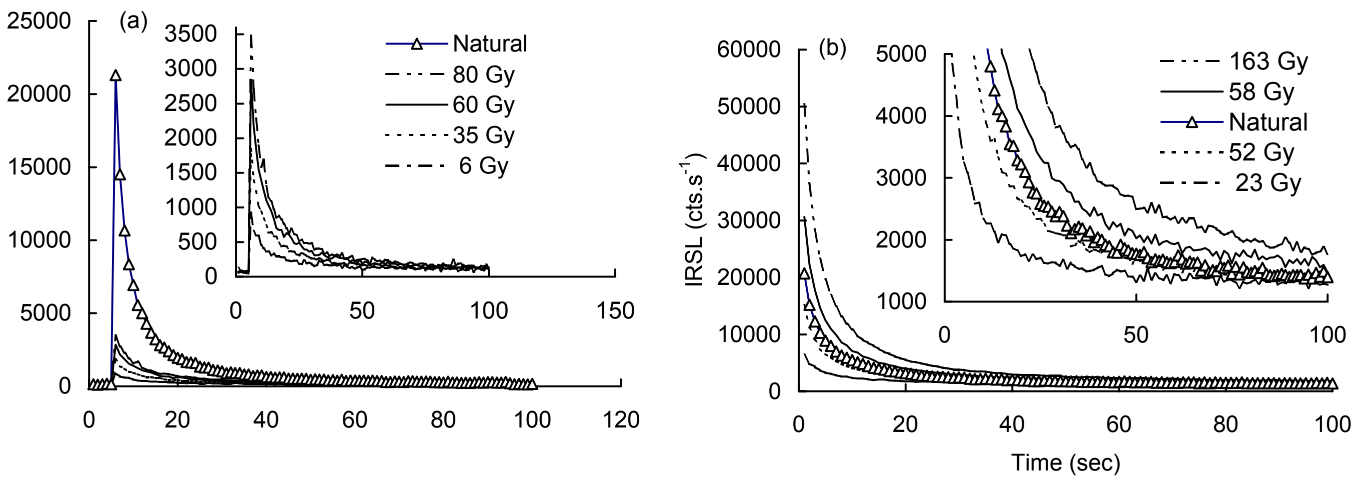

Figure 6: *Natural and laboratory red IRSL decay curves of (a) WW1A sample detected through EMI 9635Q "Blue" tube and OG 590 + BG 39. Inset shows extended y-axis scale curves. (b) 15/1 sample detected through D716A "Green" PMT and RG 665 + FR 400S + BG 39. Inset shows extended y-axis scale curves.*

Observation of the red IRSL decay form

Exposure of natural and laboratory irradiated feldspars to 830 nm IR (80% of maximum intensity) results in the prompt emission of red IRSL, which decreases to near background during the exposure of 100 seconds. Figure 5 shows the red IRSL decay curve observed for a natural feldspar sample measured at 150°C. Natural and laboratory irradiated red IRSL decay curves of samples WW1A and 21/1 are shown in Figure 6. Both curve fitting analysis of these continuous wave red IRSL decay curves and LM- red IRSL analysis indicate that the decay form is best modelled by the sum of three exponential forms with different physical properties (e.g., decay rate and saturation with dose) (Fattahi, 2001).

Red emission IRSL and Red TL sensitivity changes

To explore red emission IRSL and Red TL sensitivity changes, Fattahi (2001) examined the red IRSL decay curves and RTL (0-500ºC) glow curves of two heated potassium feldspar (OX_{OD}847/5 and 99/5/1) by repeat measurements (dose-IRSL-RTL) on samples. He demonstrated that IRSL decay curves and RTL glow curves are highly reproducible.

However, this is valid only for repeated experiments in the laboratory. For dating applications, the sensitivity change between the natural process of irradiation and the laboratory irradiation, unfortunately, can not be asserted, even if no sensitivity change has occurred in the lab.

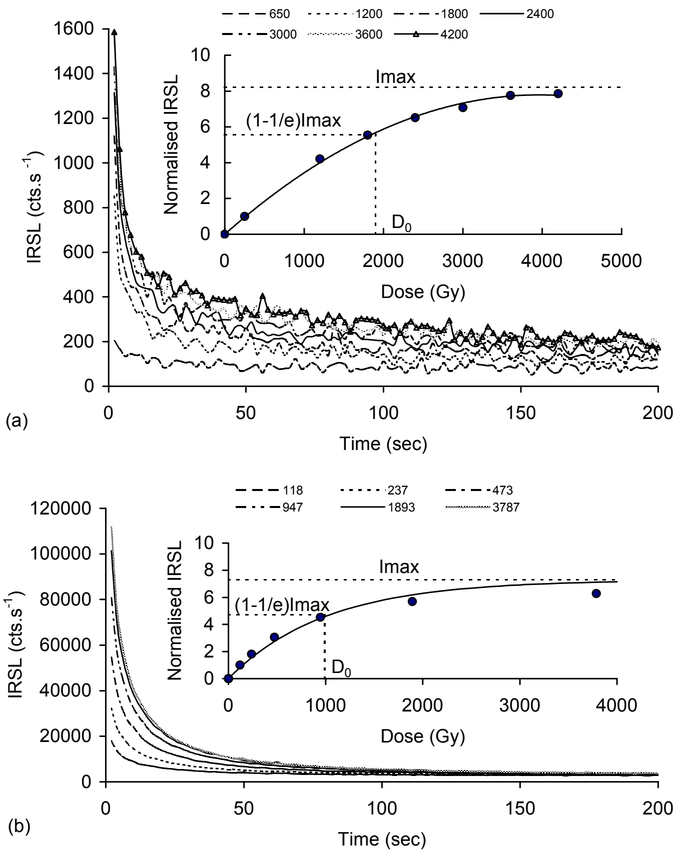

Figure 7: *Regenerated red IRSL decay curves of feldspar extracted from sample 99/5/1 and WW1A potassium feldspars. (a) Top shows the added dose in Gy for 99/5/1 sample. Inset shows the growth curves plotted for initial (first second), D_0 is the characteristic saturation dose. The detection system was D716A "Green" PMT and Omega 625. (b) The same as (a) but for far-red IRSL fromWW1A sample. The detection system was "Green" PMT and RG 665 + FR 400S + BG 39.*

Red IRSL Dose Response

An important potential advantage of red IRSL is its high dose response characteristic. We have constructed regenerated growth curves over extended dose ranges. Figure 7 summarises the red IRSL decay and growth curve data for 99/5/1 and WW1A potassium feldspar samples. The orange-near-red and far-red IRSL exhibits continued growth with doses up to 4 and 2 kGy, respectively. Using the first second of red IRSL minus the background (average of the last 5 seconds) suggests that the growth form is well modelled by a single saturating exponential. The characteristic saturation dose (D_0) for samples 99/5/1 and WW1A are 1800 and 1000Gy, respectively. If these values are taken as representing the maximum range of "easily utilized" dose, and we assume typical environmental dose rates of 1-2 $Gy.ka^{-1}$, the useable age range of the dosimeter, assuming trap stability over the same period, is in the order of 0.5-2 million years. While for these samples the dose-response data are well modelled by single saturating exponentials model, other results described elsewhere indicate that in some cases an exponential plus linear model provides a better fit.

It should be mentioned that Miallier (personal communication) has found that in some cases, for RTL of old quartz samples, the growth curve has not at all the same shape as the growth curve for samples reset in the lab. He believes that this is probably due to "ageing effects" that will take a long time to become significant (e.g., internal new traps creation under radiation, or defects diffusion) and that are annealed by heating.

The effect of measurement temperature on red IRSL signal

The effect of measurement temperature on orange-near-red and far-red IRSL was examined using sample WW1A, a potassium feldspar. Both IRSL signals showed almost identical pattern. The red IRSL signal first increased up to a sample temperature of 120°C and then decreased to a minimum close to 300°C. Here, we explain the details of the experiments that we performed. Similar experiments were performed using both detection windows.

The red IRSL decay curves of laboratory irradiated WW1A sample, which had been given a 240 Gy dose, were measured during 100 s illumination with IR, while the sample was held at temperatures from 20 to 460°C in 20°C steps (Figure 8). To observe possible phosphorescence components and any thermally stimulated contribution to the red IRSL signal, the aliquot was held at the stimulation

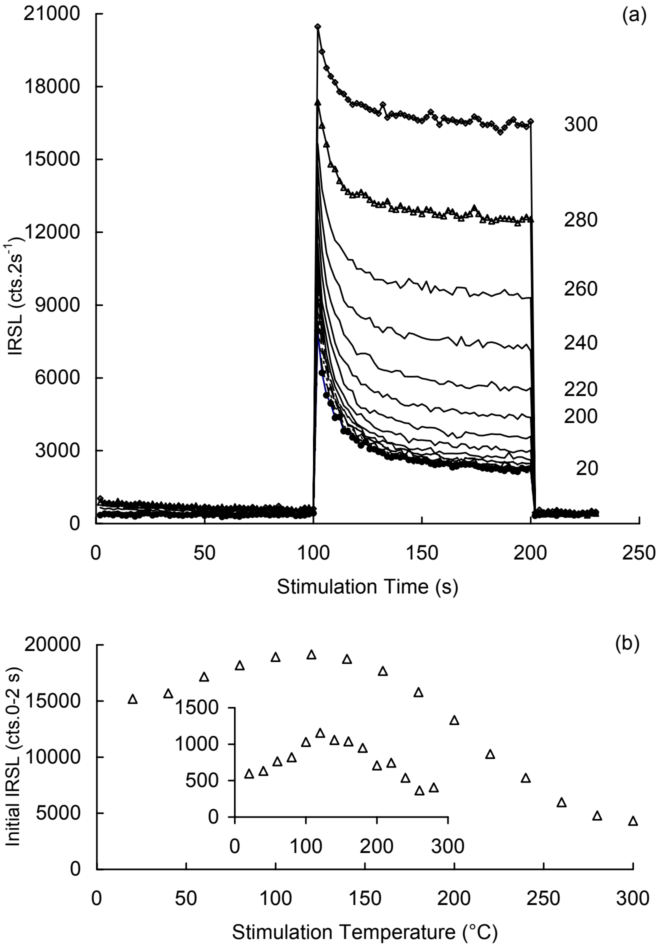

Figure 8 : *The effect of stimulation temperature on red IRSL. (a) The orange-near-red IRSL obtained for potassium feldspar (WW1A), which had been given a 240 Gy dose, before every orange-near-red IRSL measurement at elevated temperature from 20 to 460°C in 20°C steps. (b) Variation in net initial (100-102 s less background estimated from 190-200 s) laboratory irradiated orange-near-red IRSL signals obtained for 100 s at stimulation temperature (after subtracting the data without illumination from the data collected with IR) plotted versus stimulation temperature. A dose of 240 Gy was given prior to every IR stimulation (see text). Orange-near-red IRSL was observed through D716A "Green" PMT and Omega 625. Inset shows the result of similar experiment but using D716A "Green" PMT and RG 665 + FR 400S + BG 39.*

temperature for 100 seconds prior to the red IRSL measurement. After the red IRSL measurements, the luminescence was measured for 30 seconds, at the stimulation temperature but with no illumination, to observe any thermally assisted component. As can be seen in Figure 8a, increasing the temperature significantly increases the background of IRSL (100–200 s). In comparison, the thermal effect (0-100 s and 200-230 s) is very low. This difference could be explained by several possible mechanisms including increases in the IR reflection at higher sample temperatures and thermally sensitive deep traps providing electrons to IR sensitive shallower traps. This component is significantly greater than instrumental and thermal background, and was subtracted from the red IRSL measurements by subtracting the data measured with no illumination from the data measured with IR (100-200 s).

Variations in net initial (100-102 s less background estimated from 190-200 s) laboratory irradiated orange-near-red emission signals are plotted versus stimulation temperature in Figure 8b. The inset shows the result of the same experiments, using far-red IRSL signals. An initial increase by ~ 33% (for orange-near-red) and 150% (for far-red IRSL) of the original signal in the net integral between 20-120°C is followed by a decrease of ~ 66% (for orange-near-red) and ~ 50% (for far-red IRSL) compared with their original IRSL intensity between 120-300°C. Based on Figure 8b, it is advantageous to elevate sample temperature during measurement (c. 120°C). An elevated measurement temperature might additionally remove any phototransfer component in low temperature traps, as has been described in quartz OSL studies (e.g., Murray and Wintle 1998), but could additionally result in complications relating to the thermal erosion and thermal quenching of signal. In the case of orange-near-red IRSL this increase might be due to the effect of yellow peak transfer to higher wavelengths with increasing temperature (Rieser et al., 1997). These factors are discussed elsewhere (Fattahi, 2004).

Conclusions

While IRSL from feldspar has attracted considerable attention for dating applications, satisfactory agreement with independent age control for most samples has been hampered by a series of behavioural problems, in particular, anomalous fading (Duller, 1997). It is reported that RTL (>600 nm) of feldspar does not suffer from anomalous fading (Visocekas, 2000). We have systematically examined the possibility of observing red IRSL from potassium feldspar as an alternative approach. Assuming that there is a similarity in physical properties of RTL and red IRSL (as has been the case for UV-blue emission of both feldspar and quartz), the resulting signal may not exhibit anomalous fading (tested in Fattahi and Stokes, 2003c), and be suitable for dating applications (Fattahi and Stokes, 2003d).

In order to maximise red IRSL measurements, the data suggest that efficient PMT/filter combinations are of the bialkaline D716A PMT + two FR 400S, and either OG 590 or RG 665 for wide red (600-720 nm) or far red (665-720 nm), respectively. The bialkaline D716A PMT and an Omega 625DF 50 filter is the optimal combination for orange-near-red (600-660 nm).

Among the other factors controlling the signal and background are IR intensity and wavelength, substrate IR reflectivity, and measurement temperature. The major findings regarding these three give rise to the following: (1) Increasing IR intensity significantly increases both signal and background. (2) Decreasing IR (830 nm) reflectivity of substrate, can significantly decrease the background. (3) Increasing the stimulation temperature increases the signal and background. Much of the thermal incandescence can be avoided using suitable IR cut filters.

The system can easily observe red IRSL decay curves from natural and laboratory irradiated feldspars, and provides a capability of detecting red IRSL from doses as small as 6 Gy.

Preliminary investigations have shown that the red IRSL characteristics of potassium feldspars are very promising for dating applications, including reproducibility of IRSL curves, well-behaved growth curve form, and high dose saturation.

We believe that red IRSL, and particularly emissions > 665 nm, open up interesting new areas for luminescence research, which should be fully tested as an alternative to the generally poorly behaved UV-blue emission from feldspar.

Acknowledgements

Ministry of Science, Research and Technology of Iran and Tehran University kindly supported funding of MF. The authors would like to thank Alison Colls who provided some prepared potassium feldspar samples. Particular thanks are due to Ailsa Allen and David Sansom for technical support. We gratefully acknowledge Mike homer and his colleagues (Electron Tube Limited) for providing D716A PMT and technical support. We wish to thank Dr Didier Miallier for critical constructive review of the manuscript. MF gratefully acknowledges Mrs G. Fattahi for general support.

References

Aitken M.J., (1998). *An introduction to optical dating: The dating of Quaternary sediments by the use of photon-stimulated luminescence.* Oxford University Press. 267 pp.

Balescu S., Lamothe M., Auclair M.A., and Shilts W.W., (2001). IRSL dating of Middle Pleistocene interglacial sediments from southern Quebec (Canada) using multiple and single grain aliquots. *Quaternary Science Reviews* **20**, 821-824.

Clarke, M.L., Wintle, A.G. and Lancaster, N., (1996). Infra-red stimulated luminescence dating of sands from the Cronese Basins, Mojave Desert. *Geomorphology* **17**, 199-205.

Duller G.A.T., (1994a). Luminescence dating of poorly bleached sediments from Scotland. *Quaternary Science Reviews (Quaternary Geochronology)* **13**, 521-524.

Duller G.A.T., (1994b). Luminescence dating of sediments using single aliquots: new procedures. *Quaternary Science Reviews (Quaternary Geochronology)* **13**, 149-156.

Duller G.A.T., (1997). Behavioural studies of stimulated luminescence from feldspars. *Radiation Measurements* **27**, 663-694.

Fattahi M. and Stokes S., (2000). Red thermoluminescence (RTL) in volcanic quartz: development of a high sensitivity detection system and some preliminary findings. *Ancient TL* **18**, 35-44.

Fattahi, M., (2001). *Studies on red thermoluminescence and infrared stimulated red luminescence*. Unpublished D.Phil. thesis, Oxford University, Oxford.

Fattahi M., (2004). The dependence of orange-red IRSL decay curves of potassium feldspar on sample temperature. *Radiation measurements*. **38**, 287-298

Fattahi M. and Stokes S., (2001). Luminescence dating of Quaternary Volcanic events. A review of previous investigations and some observations on the potential of red luminescence emissions. *School of Geography of university of Oxford Research papers*, **58**, 1-72

Fattahi M. and Stokes S., (2003a). Dating volcanic events by luminescence. *Earth Science Reviews*. **62**, 229-264.

Fattahi M. and Stokes S., (2003b). Orange- Red IRSL in sedimentary and volcanic feldspar: development of a sensitive detection system and some preliminary findings. *Ancient TL* **21**, 25-34.

Fattahi M. and Stokes S., (2003c). Infrared stimulated red luminescence from potassium feldspar for dating applications: A study of some properties relevant for dating. *Radiation Measurements*, **37**, 647-660.

Fattahi M. and Stokes S., (2003d). Absorbed dose evaluation in feldspar using a single-aliquot regenerative-dose (SAR) infrared-stimulated red luminescence protocol. *Radiation Measurements*, **38**, 127-134.

Huntley D.J., Godfrey-Smith D.I., and Thewalt M.L.W., (1985). Optical dating of sediments. *Nature* **313**, 105-107.

Huntley D.J. and Lamothe M., (2001). Ubiquity of anomalous fading in K - feldspar and the measurement and correction for it in optical dating. *Canadian Journal of Earth Sciences* **38**, 1093-1106.

Hütt G., Jaek I., and Tchonka J., (1988). Optical dating: potassium feldspars optical response stimulation spectra. *Quaternary Science Reviews* **7**, 381-385.

Krbetschek M.R., Götze J., Dietrich A., and Trautmann T., (1997). Spectral information from minerals relevant for luminescence dating. *Radiation Measurements* **27**, 695-748.

Lamothe M. and Auclair M., (1997). Assessing the datability of young sediments by IRSL using an intrinsic laboratory protocol. *Radiation Measurements* **27**, 107-117.

Lamothe M. and Auclair M., (1999). A solution to anomalous fading and age shortfalls in optical dating of feldspar minerals. *Earth and Planetary Science Letters* **171**, 319-323.

Lamothe M. and Auclair M., (2000). The fadia method: a new approach in luminescence dating using the analysis of single feldspar grains. *Radiation Measurements* **32**, 433-438.

Li S. H. and Wintle A.G., (1994). Use of infra-red stimulated luminescence signals from pellets of compressed loess from Rocourt, Belgium. *Quaternary Science Reviews (Quaternary Geochronology)* **13**, 529-532.

Lian O.B. and Shane P.A., (2000). Optical dating of paleosols bracketing the widespread Rotoehu tephra, North Island, New Zealand. *Quaternary Science Reviews* **19**, 1649-1662.

Murray A.S. and Wintle A.G., (1998). Factors controlling the shape of the OSL decay curve in quartz. *Radiation Measurements* **29**, 65-79.

Poolton N.R.J., Bøtter-Jensen L., and Duller G.A.T., (1995). Thermal quenching of luminescence processes in feldspars. *Radiation Measurements* **24**, 57-66.

Poolton N.R.J., Wallinga, J., Murray, A.S., Bulur, E. and Bøtter-Jensen, L., (2002a). Electrons in feldspar I: on the wavefunction of electrons trapped at simple lattice defects. *Physics and Chemistry of Minerals* **29**, 210-216

Poolton, N.R.J., Ozanyan, K. B., Wallinga, J., Murray, A.S. and Bøtter-Jensen, L, (2002b). Electrons in feldspar II: a consideration of the influence of conduction band-tail states on luminescence processes. *Physics and Chemistry of Minerals* **29**, 217-225

Richardson C.A., McDonald E.V., and Busacca A.J., (1997). Luminescence dating of loess from the northwest United States. *Quaternary Science Reviews* **16**, 403-415.

Richardson C.A., Mcdonald E.V., and Busacca A.J., (1999). A luminescence chronology for loess deposition in Washington State and Oregon, USA. *Zeitschrift fur. Geomorphologie. N.F.* **116**, 77-95.

Rieser, U. Hütt, G. Krbetschek M. R. and Stolz, W., (1997). Feldspar IRSL emission spectra at high and low temperatures; *Radiation Measurements*, **27**, 273-278.

Spooner N.A., (1992). Optical dating: Preliminary results on the anomalous fading of luminescence from feldspars. *Quaternary Science Reviews* **11**, 139-145.

Spooner N.A., (1994). The anomalous fading of infrared-stimulated luminescence from feldspars. *Radiation Measurements* **23**, 625-632.

Trautmann, T., Krbetschek, M.R. Dietrich A. and Stolz, W., (2000). The basic principle of radioluminescence dating and a localized transition model, *Radiation Measurements* **32**, 487-492

Visocekas R., (2000). Monitoring anomalous fading of TL of feldspars by using far-red emission as a gauge. *Radiation Measurements* **32**, 499-504.

Wallinga, J., Murray, A.S. and Duller, G.A.T., (2000). Underestimation of equivalent dose in single-aliquot optical dating of feldspars caused by preheating. *Radiation Measurements*, **32**, 691-695.

Wintle A.G., (1997). Luminescence dating: laboratory procedures and protocols. *Radiation Measurements* **27**, 769-818.

Zink A.J.C. and Visocekas R., (1997). Datability of sanidine feldspars using the near-infrared TL emission. *Radiation Measurements* **27**, 251-261.

Reviewer
Didier Miallier

The dose rate of beta sources for optical dating applications: A comparison between fine silt and fine sand quartz

Barbara Mauz and Andreas Lang

Department of Geography, University of Liverpool, Liverpool L69 7ZQ, United Kingdom

(Received 11 January 2005; in final form 18 January 2005)

Abstract

This note reports on the determination of the dose rates of beta sources used for optical dating. Equipment and targets used for the experiments were chosen according to dating application requirements: sand-sized and silt-sized quartz mounted on aluminium and stainless-steel discs were measured in two Risø readers using a single aliquot regeneration dose protocol.

The experiments show that backscattering due to disc substrate accounts for ~ 16% of the dose rate. Charge build-up and attenuation associated with the grain size of the target accounts for ~ 11% of the dose rate. The total uncertainty of the dose rates is ~ 2% or less depending on the accuracy of the primary gamma-source. The excellent agreement between our values and those reported by Armitage and Bailey (2005) indicate that factors determined can be adopted by other laboratories.

Introduction

One of the most crucial laboratory parameters for optical dating applications is the dose rate of the beta source used to reconstruct the environmental dose experienced by a sample. The dose given to quartz during laboratory beta irradiation depends on charge build-up, attenuation and backscattering (Aitken, 1985). While charge build-up and attenuation depends on the mineral and its grain size, backscattering is a function of the sample carrier (disc). Maintaining backscattering constant, Wintle and Aitken (1977) reported a ~ 25% lower dose rate for 4-11µm samples than for ~ 100 µm samples. Armitage and Bailey (2005) show that ~ 12% of the beta dose rate is derived from the grain size of the target. The enormous difference between ~ 25% and 12% is due to differences in measurement protocols and geometry. The sample-to-source distance decreased from ~ 16 mm (Wintle and Aitken, 1977) to ~ 7 mm (Markey et al., 1997) and, thus, the maximum angle at which the beta particles hit the sample and the build-up effect are changed.

The purpose of this note is to describe our approach of assessing beta source dose rates and to compare our results with those of Armitage and Bailey (2005).

Experimental details

Materials, discs and aliquot sizes:

1. Sand-sized quartz (150-250 µm) provided by the Risø National Laboratory. The sample has the laboratory number 914807 and was irradiated on 16.08.1999. The grains were mounted on aluminium and stainless-steel discs using silicone oil. Each aliquot contained ~1500 grains. These grains covered the inner 7-7.5 mm of discs of 9.7±1 mm diameter.

2. Silt-sized quartz (10-20 µm) provided by the Liverpool Luminescence Laboratory. The material was settled on aluminium discs using acetone. Each aliquot contained 2.5 mg material, which covered the entire 9.7±1 mm diameter discs.

The silt-sized quartz was extracted from loess sediment originating from the “Nussloch-site” in southern Germany. The loess sample was treated using the conventional procedures for fine grain samples, etched in 20% hydrofluoric acid for several tens of minutes until tests (Mauz and Lang, 2004) showed its quartz purity. The material was then washed in acetone, dried and settled in acetone onto aluminium discs. The aliquots were then annealed at 500°C for 1 hour and subsequently sensitized in the Risø reader by alternating irradiation (~5 Gy) and OSL read-out (40 s at 125°C) 18 times. The sensitized material was subsequently washed off the discs and sent to the National Physical Laboratory (NPL) for gamma-irradiation. After gamma-irradiation the sample was again settled onto aluminium discs and stored for around 6 weeks at room temperature before measurement.

γ-dose (Gy)	Grain size range (μm)	Position in wheel	Disc	$D_{eß}$ (s)	Recycling ratio
$^{90}Sr/^{90}Y$ source mounted on Risø DA 15B/C					
4.59±0.07	150-250	1	ss	34.68±2.76	1.00±0.003
4.59±0.07	150-250	8	ss	34.86±2.13	0.996±0.002
4.59±0.07	150-250	20	ss	34.58±1.83	1.004±0.002
4.59±0.07	150-250	32	ss	34.65±2.77	1.003±0.007
4.59±0.07	150-250	43	ss	34.65±2.35	1.009±0.003
4.59±0.07	150-250	1	al	40.11±2.80	0.989±0.003
4.59±0.07	150-250	8	al	40.54±2.70	0.988±0.003
4.59±0.07	150-250	20	al	39.76±2.92	1.021±0.004
4.59±0.07	150-250	32	al	41.05±2.98	1.008±0.003
4.59±0.07	150-250	43	al	41.83±3.51	1.016±0.002
8.92±0.18	10-20	1	al	88.13±4.35	1.0184±0.0005
8.92±0.18	10-20	8	al	89.27±5.04	1.0274±0.0003
8.92±0.18	10-20	20	al	88.59±3.99	1.0143±0.0003
8.92±0.18	10-20	32	al	89.41±5.71	1.0307±0.0003
8.92±0.18	10-20	43	al	89.37±4.10	1.0169±0.0003
$^{90}Sr/^{90}Y$ source mounted on Risø DA15					
4.59±0.07	150-250	1	ss	45.00±2.12	1.001±0.003
4.59±0.07	150-250	8	ss	45.32±3.10	0.972±0.007
4.59±0.07	150-250	20	ss	45.52±3.63	0.97±0.02
4.59±0.07	150-250	32	ss	44.92±2.36	0.99±0.01
4.59±0.07	150-250	43	ss	45.91±3.51	0.998±0.001
4.59±0.07	150-250	1	al	53.93±4.23	1.006±0.003
4.59±0.07	150-250	8	al	51.71±2.28	0.991±0.002
4.59±0.07	150-250	20	al	51.49±4.15	1.016±0.010
4.59±0.07	150-250	32	al	51.86±3.95	1.010±0.006
4.59±0.07	150-250	43	al	52.51±2.80	1.030±0.002
8.92±0.18	10-20	1	al	114.56±7.57	1.007±0.005
8.92±0.18	10-20	8	al	113.51±9.00	1.008±0.006
8.92±0.18	10-20	20	al	115.43±7.91	1.000±0.005
8.92±0.18	10-20	32	al	110.80±13.29	1.006±0.005
8.92±0.18	10-20	43	al	113.54±12.46	1.003±0.005

Table 1 : *Beta equivalent doses ($D_{eß}$ ± standard error, in seconds irradiation time) of individual aliquots and parameters associated. ss stands for stainless-steel and al for aluminium; recycling ratio is the ratio of the first regenerated dose and the repeated first regenerated dose at the end of the SAR protocol. All errors are quoted at 1σ.*

Risø reader	Grain size range (μm)	Disc	Dose rate (Gy s^{-1})	Uncertainty (%)	Normalized dose rate
DA15	150-250	stainless-steel	0.101±0.002	1.6	1.00
DA15	150-250	aluminium	0.088±0.001	1.6	0.87
DA15	10-20	aluminium	0.0785±0.002	2.1	0.78
DA15B/C	150-250	stainless-steel	0.132±0.002	1.5	1.00
DA15B/C	150-250	aluminium	0.113±0.002	1.5	0.86
DA15B/C	10-20	aluminium	0.100±0.002	2.0	0.76

Table 2: *Dose rates of the beta sources examined and their dependence on grain size and substrate of disc. Normalised dose rates were normalised to the stainless steel values to facilitate comparison. All errors are quoted at 1σ.*

Gamma sources and given γ-doses
Risø used a ^{137}Cs source (662 keV in air) delivering 0.1013±0.0012 Gy hour^{-1} (20/5/98), while NPL used a ^{60}Co source (1.25 MeV in water) delivering 0.949 Gy min^{-1} (7/9/2004). The sand-sized quartz received a dose of 4.59±0.07 Gy. The silt-sized quartz received a dose of 8.92±0.18 Gy.

Measurement equipment
One reader is a Risø DA-15 equipped with 41 blue LEDs (Nichia NSPB 500S) emitting 470Δ30 nm and an EMI 9235QB photomultiplier. The ß-source mounted on this reader is a ~4 years old 40 mCi ^{90}Sr/^{90}Y source and the source-to-sample distance is 7.4 mm. The second reader is a Risø DA-15B/C equipped with 27 blue LEDs (Nichia NSPB 500S) emitting 470Δ30 nm. In terms of construction and housing its ß-source is identical to the first one (Markey et al., 1997 and Bøtter-Jensen et al., 2000); it is around one year old and the source-to-sample distance is 5 mm (Bøtter-Jensen et al., 2000). The optical stimulation units of both readers deliver ~ 30 mW cm^{-2} at 90% power. For detection a 7.5 mm Hoya U340 filter transmitting 290-380 nm was used in each reader.

Experimental design
The wheel used as an aliquot carrier in the Risø reader is a 6.0 mm to 6.1 mm thick aluminium ring. During manufacturing the wheel experiences stress which results in a slight bending of a regular pattern, shown by a dial-test indicator. With respect to the reference surface the wheel shows zero elevation at positions 1-5, 13-18, 23-28 and 36-42. At positions 19-22 and 43-48 a –40 μm depression was measured and at positions 6-12 and 30-35 a +60 μm and +40 μm height respectively was recorded using a depth micrometer. Thus, there is a height amplitude of maximum 100 μm between positions 6-12 and 19-22. We have chosen the following positions on the wheel for our experiments: 1, 8, 20, 32, 43. A single aliquot regeneration dose protocol (SAR) was used to recover the given gamma dose with 260°C for 10 s as a preheat, heating to 200°C as a cut heat, and 40 s illumination with blue LEDs (90% power) at 125°C for OSL recording.

Experimental uncertainties
Uncertainties resulted from: (i) γ-irradiation: photon mass-energy absorption at 662 keV (Risø) and 1.25 MeV (NPL), photon fluence perturbation due to the sample carrier and mass absorption of quartz to air and water, respectively. The uncertainty of the dose to quartz provided by the Risø National Laboratory was 1.5% and that of the NPL was 2%. (ii) SAR protocol performed in Risø readers. We adopted a 1.5% systematic error (following Armitage et al., 2000) in addition to the standard error given by the arithmetical mean of 5 aliquots in each measurement. The shortest irradiation time was 32 s, which allows us to disregard a systematic error related to the irradiation time.

Results and discussion
The data resulting from the two experiments are shown in Table 1. Table 2 indicates the dose rates in dependence of grain size and sample carrier. The uncertainty of the beta equivalent doses resulting from the SAR protocol was ~ 6% per aliquot and, thus, obscured any differences between positions in the wheel. For sand-sized samples the factor between stainless-steel discs and aluminium discs is 1.16±0.01. Assuming that the difference in thickness between the two disc types is negligible, the disc material itself accounts for around 16% dose rate of the ß-source. This result confirms not only that steel discs produce higher backscattering and enhance the beta dose rate, it is also in agreement with the 14%

difference reported by Ingram et al. (2001) and the 16.6±0.2% published by Armitage and Bailey (2005). The factor between silt-sized and sand-sized quartz samples mounted on aluminium discs is 0.89±0.005 and thus, the grain size accounts for around 11% dose rate of the ß-source. This result again, confirms Armitage and Bailey (2005) who analysed the beta dose rate dependence on grain size. These authors report a maximum difference between sand- and silt-sized quartz of ~12%. Within the 1σ uncertainty level both Risø readers gave the same results indicating that a few millimetres difference in sample-to-source distances does not affect the factors determined.

The total uncertainty of the dose rates determined is ~1.6% for sand-sized quartz and ~2% for silt-sized quartz. The small difference of ~0.4% is due to the uncertainty derived from the γ-source.

The standard aliquot size used in this experiment is 7 mm. This size allows us to adopt the dose rate factors reported by Spooner and Allsop (2000) to correct the mean total dose rate received by the standard aliquot size to smaller and larger aliquot sizes.

Conclusion

While the effect of backscattering on beta source dose rates was known from previous studies, the dependence of the dose rate on grain sizes was only assumed when our study started. We now find an excellent agreement between our results and those of Armitage and Bailey (2005). This agreement indicates that the factors determined between aluminium and steel discs on the one hand and sand-sized and silt-sized quartz on the other can be adopted by other laboratories.

Acknowledgements

We thank Ian Stoker and James Manning from the National Physical Laboratory for performing the gamma irradiation and calculating the dose given to the silt-sized quartz sample. We further thank S. Packman for reviewing the manuscript.

References

Aitken, M. J. (1985). *Thermoluminescence dating*. Academic Press, London, 378pp.

Armitage, S.J. and Bailey, R.M. (2005). The measured dependence of laboratory beta dose rates on sample grain size. *Radiation Measurements* **39**, 123-127.

Armitage, S.J., Duller, G.A.T. and Wintle, A.G. (2000). Quartz from South Africa: sensitivity changes as a result of thermal pretreatment. *Radiation Measurements* **32**, 571-577.

Bøtter-Jensen, L., Bulur, E., Duller, G.A.T. and Murray, A.S. (2000). Advances in luminescence instrument systems. *Radiation Measurements* **32**, 523-528.

Ingram, S., Stokes, S. and Bailey, R. (2001). Confirmation of backscattered beta dose enhancement rates based on single aliquot regeneration (SAR) analysis of quartz sand and silt. *Ancient TL* **19**, 51-54.

Markey, B.G., Bøtter-Jensen, L., Duller G.A.T. (1997). A new flexible system for measuring thermally and optically stimulated luminescence. *Radiation Measurements 27, 83-89.*

Mauz, B. and Lang, A. (2004). Removal of the feldspar-derived luminescence component from polymineral fine silt samples for optical dating applications: evaluation of chemical treatment protocols and quality control procedures. *Ancient TL* **22**, 1-8.

Spooner, N. A. and Allsop, A. (2000). The spatial variation of dose-rate from $^{90}Sr/^{90}Y$ beta sources for use in luminescence dating. *Radiation Measurements* **32**, 49-56.

Wintle, A.G. and Aitken, M.J. (1977). Absorbed dose from a beta source as shown by thermoluminescence dosimetry. *Int. J. Appl. Radiat. Isot.* **28**, 625-627.

Reviewer

Richard Bailey

Thesis Abstract

Author: Anette Engelmann
Thesis Title: Aeolianites and palaeosols in Israel: Luminescence chronology and relationship with eastern Mediterranean climates
Grade: PhD
Date: January 2004
Supervisor: Frank Chambers and Manfred Frechen
Address: University of Gloucestershire, Cheltenham

Aeolianites and palaeosols on the Mediterranean coastal plains of Israel were investigated with luminescence dating in order to explore the sedimentological evidence for climate change in the area and the response to it.

The dated samples were taken from sites between the towns of Haifa and Netanya South, which are located in a quarry near the town of Habonim and further towards the coast, in a quarry North of the town of Hadera and further towards the coast as well as at the coastal cliff and in a sewage gully by the town of Netanya South.

The aims of this study were to correlate aeolianite and palaeosol exposures along the Mediterranean coast, to establish a chronology for a climatological interpretation, and also whether aeolianite formation and palaeosol development could be correlated with major climate events of the Late Pleistocene in the Eastern Mediterranean.

Over 80 samples were collected from various sites, covering exposures from North to South and also from East to West. They were dated with infrared optical stimulated luminescence (IR-OSL) and thermoluminescence (TL). In addition radio-fluorescence spectra were obtained from some of the samples and also their equivalent doses were determined with infrared radiofluorescence (IR-RF).

The chronology established through the luminescence dating results showed that aeolianite formation and palaeosol development in the Carmel and Sharon coastal plains are connected with the cyclical occurrence of enhanced rainfall over the Mediterranean. These conditions, which also cause the Mediterranean sapropels to form, are characterised by a sudden increase of precipitation. The rainfall lessens over the time of the episode but temperatures increase. It is likely that most of the soils in the coastal plains developed during the humid conditions of the rainfall episodes, while sand accumulation and aeolianite formation took place during the arid conditions at the end of the rainfall episodes or shortly afterwards. A new climate-event-stratigraphical model for the correlation of the deposits is suggested.

Bibliography
Compiled by Ann Wintle

From 1st October 2004 to 31st December 2004

Adamiec, G. (2005). Investigation of a numerical model of the pre-dose mechanism in quartz. *Radiation Measurements* **39,** 179-189.

Adamiec, G. (2005). OSL decay curves - relationship between single- and multiple-grain aliquots. *Radiation Measurements* **39,** 63-75.

Adamiec, G. (2005). Properties of the 360 and 550 nm TL emissions of the "110 C peak" in fired quartz. *Radiation Measurements* **39,** 105-110.

Armitage, S. J., and Bailey, R. M. (2005). The measured dependence of laboratory beta dose rates on sample grain size. *Radiation Measurements* **39,** 123-127.

Attanasio, D., Platania, R., and Rocchi, P. (2005). White marbles in Roman architecture: electron paramagnetic resonance identification and bootstrap assessment of the results. *Journal of Archaeological Science* **32,** 311-319.

Bailiff, I. K., Stepanenko, V. F., Göksu, H. Y., Jungner, H., Balmukhanov, S. B., Balmukhanov, T. S., Khamidova, L. G., Kisilev, V. I., LKolyado, I. B., Kolizhenkov, T. V., Shoikhet, Y. N., and Tsyb, A. F. (2004). The application of retrospective luminescence dosimetry in areas affected by fallout from the Semipalatinsk nuclear test site: an evaluation of potential. *Health Physics* **87,** 625-641.

Beerten, K., and Stesmans, A. (2005). Single quartz grain electron spin resonance (ESR) dating of a contemporary desert surface deposit, Eastern Desert, Egypt. *Quaternary Science Reviews* **24,** 223-231.

Bowman, D., Korjenkov, A., Porat, N., and Czassny, B. (2004). Morphological response to Quaternary deformation at an intermontane basin piedmont, the northern Tien Shan, Kyrghyzstan. *Geomorphology* **63,** 1-24.

Cannas, M., Agnello, S., Boscaino, R., Gelardi, F. A., and Trukhin, A. (2004). Photoluminescence in gamma-irradiated alpha-quartz investigated by synchrotron radiation. *Radiation Measurements* **38,** 507-510.

De Corte, F., Vandenberghe, D., Hossain, S. M., De Wispelaere, A., and Van den Haute, P. (2004). The effect of different sample-calibrant composition in gamma-ray spectrometry for the assessment of the radiation dose rate in the luminescence dating of sediments. *Journal of Radioanalytical and Nuclear Chemistry* **262,** 261-267.

Eitel, B., Kadereit, A., Blümel, W. D., Hüser, K., and Kromer, B. (2005). The Amspoort Silts, northern Namib desert (Namibia): formation, age and palaeoclimatic evidence of river-end deposits. *Geomorphology* **64,** 299-314.

Finch, A. A., Garcia-Guinea, J., Hole, D. E., Townsend, P. D., and Hanchar, J. M. (2004). Ionoluminescence of zircon: rare earth emissions and radiation damage. *Journal of Physics D - Applied Physics* **37,** 2795-2803.

Galbraith, R. F., Roberts, R. G., and Yoshida, H. (2005). Error variation in OSL palaeodose estimates from single aliquots of quartz: a factorial experiment. *Radiation Measurements* **39,** 289-307.

Havholm, K. G., Ames, D. V., Whittecar, G. R., Wenell, B. A., Riggs, S. R., Jol, H. M., Berger, G. W., and Holmes, M. A. (2004). Stratigraphy of back-barrier coastal dunes, northern North Carolina and Southern Virginia. *Journal of Coastal Research* **20,** 980-999.

Inoue, K., Nagatomo, T., and Ikeya, M. (2005). Infrared stimulated luminescence in quartz. *Radiation Measurements* **39,** 191-196.

Jain, M., Murray, A. S., Bøtter-Jensen, L., and Wintle, A. G. (2005). A single-aliquot regenerative-dose method based on IR bleaching of the fast OSL component in quartz. *Radiation Measurements* **39,** 309-318.

Jain, M., Tandon, S. K., and Bhatt, S. C. (2004). Late Quaternary stratigraphic development in the lower Luni, Mahi and Sabarmati river basins, western India. *Proceedings of the Indian Academy of Sciences - Earth and Planetary Sciences* **113,** 453-471.

Jain, M., Tandon, S. K., Singhvi, A. K., Mishra, S., and Bhatt, S. C. (2005). Quaternary alluvial stratigraphic development in a desert setting: a case study from Luni river basin, Western India. *In* "Fluvial Sedimentology VII." (B. M., and S. Marriott, Eds.), pp. 349-371. International Association of Sedimentologists.

Juyal, N., Chamyal, L. S., Bhandari, S., Maurya, D. M., and Singhvi, A. K. (2004). Environmental changes during Late Pleistocene in the Orsang River Basin, western India. *Journal of the Geological Society of India* **64,** 471-479.

Juyal, N., Pant, R. K., Basavaiah, N., Yadava, M. G., Saini, N. K., and Singhvi, A. K. (2004). Climate and seismicity in the higher Central Himalaya during 20-10 ka: evidence from the Garbayang basin, Uttaranchal, India. *Palaeogeography, Palaeoclimatology, Palaeoecology* **213,** 315-330.

Kale, V. S., Gupta, A., and Singhvi, A. K. (2004). Late Pleistocene-Holocene palaeohydrology of monsoon Asia. *Journal of the Geological Society of India* **64,** 403-417.

Kemp, R. A., King, M., Toms, P., Derbyshire, E., Sayago, J. M., and Collantes, M. M. (2004). Pedosedimentary development of part of a Late Quaternary loess-palaeosol sequence in northwest Argentina. *Journal of Quaternary Science* **19,** 567-576.

Liritzis, I., Galloway, R. B., Hong, D., and Kyparissi-Apostolika, N. (2002). OSL dating of three prehistoric ceramics from Theopetra cave, Greece: a case study. *Mediterranean Archaeology and Archaeometry* **2,** 35-43.

Lu, H. Y., Wang, X. Y., An, Z. S., Miao, X. D., Zhu, R. X., Ma, H. Z., Li, Z., Tan, H. B., and Wang, X. Y. (2004). Geomorphologic evidence of phased uplift of the northeastern Qinghai-Tibet Plateau since 14 million years ago. *Science in China Series D Earth Sciences* **47,** 822-833.

Magee, J. W., Miller, G. H., Spooner, N. A., and Questiaux, D. (2004). Continuous 150 k.y. monsoon record from Lake Eyre, Australia; Insolation forcing implications and unexpected Holocene failure. *Geology* **32,** 885-888.

Morwood, M. J., Soejono, R. P., Roberts, R. G., Sutikna, T., Turney, C. S. M., Westaway, K. E., Rink, W. J., Zhao, J. X., van den Bergh, G. D., Due, R. A., Hobbs, D. R., Moore, M. W., Bird, M. I., and Fifield, L. K. (2004). Archaeology and age of a new hominin from Flores in eastern Indonesia. *Nature* **431,** 1087-1091.

Nasdala, L., Gotze, J., Hanchar, J. M., Gaft, M., and Krbetschek, M. R. (2004). Luminescence techniques in Earth Sciences. *In* "Spectroscopic methods in mineralogy." (A. Beran, and E. Libowitzky, Eds.), pp. 43-71. Eotvos University Press, Budapest.

Preusser, F., and Schluchter, C. (2004). Dates from an important early Late Pleistocene ice advance in the Aare valley, Switzerland. *Ecologae Geologicae Helvetiae* **97,** 245-253.

Radies, D., Preusser, F., Matter, A., and Mange, M. (2004). Eustatic and climatic controls on the development of the Wahiba Sand Sea, Sultinate of Oman. *Sedimentology* **51,** 1359-1385.

Rasheedy, M. S. (2004). An independent method for obtaining the activation energy of thermoluminescence glow peaks. *International Journal of Modern Physics B* **18,** 2877-2885.

Short, M. A. (2004). Determining the possible lattice sites of two unknown defects in orthoclase from the polarization effects in their optical transitions. *Journal of Physics - Condensed Matter* **16,** 7405-7417.

Short, M. A. (2005). The simultaneous measurement of luminescence and photocurrent of an irradiated K-feldspar excited with 1.45 or 2.41 eV photons. *Radiation Measurements* **39,** 197-201.

Singhvi, A. K., and Kar, A. (2004). The aeolian sedimentation record of the Thar desert. *Proceedings of the Indian Academy of Sciences - Earth and Planetary Sciences* **113,** 371-401.

Tanir, G., Meric, N., Aytekin, H. S., and Okuducu, E. (2004). A fitting procedure for palaeodose from old sandstone using IRSL. *Czechoslovak Journal of Physics* **54,** 941-946.

Thomsen, K. J., Murray, A. S., and Bøtter-Jensen, L. (2005). Sources of variability in OSL dose measurements using single grains of quartz. *Radiation Measurements* **39,** 47-61.

Vorona, I. P., Ishchenko, S. S., and Baran, N. P. (2005). The effect of thermal treatment on radiation-induced EPR signals in tooth enamel. *Radiation Measurements* **39,** 137-141.

Zacharias, N., Buxeda i Garrigós, J., Mommsen, H., Schwedt, A., and Kilikoglou, V. (2005). Implications of burial alterations on luminescence dating of archaeological ceramics. *Journal of Archaeological Science* **32,** 49-57.

Workshop Announcement

Department of Radioisotopes
Institute of Physics, Silesian University of Technology
GADAM Centre
Gliwice Absolute Dating Methods Centre

14C OSL
PHYSICS IN EARTH SCIENCES
ENVIRONMENT AND ARCHAEOLOGY

3rd Workshop on Methods of Absolute Chronology

"Isotope methods in environmental studies"

1-6 May 2005
Ustroń, Poland

The Centre of Excellence GADAM would like to invite you to participate in the third workshop on methods of absolute chronology entitled *"Isotope methods in environmental studies"*. The workshop will provide a better insight into different aspects of applying isotope methods in environmental and palaeoenvironmental studies and their relation to methods of absolute chronology.

The workshop will consist of lectures by high-class professionals, work sessions and discussions. (To see the list of lecturers and participants in the two previous workshops follow the links under http://www.carbon14.pl/conference/). The workshop is directed mainly to PhD students and young scientists from the fields of earth sciences, archaeology and related areas.

There are awards for fifteen participants to cover the total cost of participation and travel.

The workshop will take place in the hotel "Tulipan" in Ustroń, southern Poland. To obtain more information and register please visit the webpage which can be viewed at the following web page http://www.carbon14.pl/conference/2005may/. If you have any queries about the workshop then please write to GADAM@carbon14.pl

A. Bluszcz

Announcement

Ludwig Zöller's habilitation thesis on-line

The habilitation thesis by Ludwig Zöller under the title "Stratigraphy of Würm and Riss Loess and Thermoluminescence Dating in Southern Germany and Neighbouring Areas" was submitted to the Geoscience Faculty of University of Heidelberg, Germany, in 1994 under the German title Würm- und Rißlöß-Stratigraphie und Thermolumineszenz-Datierung in Süddeutschland und angrenzenden Gebieten and was accepted by the faculty in 1995.

After the LED conference in Rome an epilogue was attached to the original manuscript. For publication planned in the series "Relief - Boden - Palaeoklima" (Relief - Soil - Palaeoclimate) an extended English abstract (pp 207-221) was added, too, together with English figure and table captions (45 figures, 3 tables), but publication failed for financial reasons. Many of the data have not been published elsewhere and are now made available to the community.

A full download as a Word document is now available on-line at the following address www.uni-bayreuth.de/departments/geomorph/docs/HABIL96rev_o.DOC

L. Zöller